



Targeting glutaminase 1 attenuates stemness properties in hepatocellular carcinoma by increasing reactive oxygen species and suppressing Wnt/beta-catenin pathway

Binghua Li^a, Yajuan Cao^a, Gang Meng^{a,b}, Liyuan Qian^a, Tiancheng Xu^a, Chen Yan^a, Ouyang Luo^a, Shaohu Wang^a, Jiwu Wei^{b,*}, Yitao Ding^{a,*}, Decai Yu^{a,*}

^a Department of Hepatobiliary Surgery, the Affiliated Drum Tower Hospital, Medical School of Nanjing University, Nanjing, 210008, China

^b Jiangsu Key Laboratory of Molecular Medicine, Medical School of Nanjing University, Nanjing, 210093, China

ARTICLE INFO

Article history:

Received 29 August 2018

Received in revised form 29 November 2018

Accepted 29 November 2018

Available online 13 December 2018

Keywords:

Glutaminase 1

Glutamine metabolism

Cancer stem cell

Stemness

Wnt/ β -catenin signaling pathway

Hepatocellular carcinoma

ABSTRACT

Background: Hepatocellular carcinoma (HCC) is an aggressive malignant disease with poor prognosis. Recent advances suggest the existence of cancer stem cells (CSCs) within liver cancer, which are considered to be responsible for tumor relapse, metastasis, and chemoresistance. However, novel therapeutic approaches for eradicating CSCs are yet to be established. Here, we aimed to identify the role of glutaminase 1 (GLS1) in stemness, and the feasibility that GLS1 serves as a therapeutic target for elimination CSCs as well as the possible mechanism.

Methods: Publicly-available data from the Cancer Genome Atlas (TCGA) and Gene Expression Omnibus (GEO) was mined to unearth the association between GLS1 and stemness phenotype. Using big data, human tissues and multiple cell lines, we gained a general picture of GLS1 expression in HCC progression. We generated stable cell lines by lentiviral-mediated overexpression or CRISPR/Cas9-based knockout. Sphere formation assays and colony formation assays were employed to analyze the relationship between GLS1 and stemness. A series of bioinformatics analyses and molecular experiments including qRT-PCR, immunoblotting, flow cytometry, and immunofluorescence were employed to investigate the role of GLS1 in regulating stemness *in vitro* and *in vivo*.

Findings: We observed GLS1 (both KGA and GAC isoform) is highly expressed in HCC, and that high expression of GAC predicts a poor prognosis. GLS1 is exclusively expressed in the mitochondrial matrix. Upregulation of GLS1 is positively associated with advanced clinicopathological features and stemness phenotype. Targeting GLS1 reduced the expression of stemness-related genes and suppressed CSC properties *in vitro*. We further found GLS1 regulates stemness properties *via* ROS/Wnt/ β -catenin signaling and that GLS1 knockout inhibits tumorigenicity *in vivo*.

Interpretation: Targeting GLS1 attenuates stemness properties in HCC by increasing ROS accumulation and suppressing Wnt/ β -catenin pathway, which implied that GLS1 could serve as a therapeutic target for elimination of CSCs.

© 2018 The Authors. Published by Elsevier B.V. This is an open access article under the CC BY-NC-ND license (<http://creativecommons.org/licenses/by-nc-nd/4.0/>).

Abbreviations: GLS1, Glutaminase 1; CSC, Cancer stem cell; ROS, Reactive oxygen species; OXPHOS, Oxidative phosphorylation; TCA, Tricarboxylic acid; TCGA, the Cancer Genome Atlas; GEO, Gene Expression Omnibus; HCC, Hepatocellular carcinoma; IHC, Immunohistochemistry; GSH, Glutathione; NADPH, Nicotinamide adenine dinucleotide phosphate; Gln, Glutamine; OMM, Outer mitochondrial membrane; IMM, Inner mitochondrial membrane; GCLC, Glutamate-Cysteine Ligase Catalytic Subunit; NAC, N-Acetyl-L-cysteine; α -KG, α -ketoglutarate; DM- α -KG, Dimethyl 2-oxoglutarate.

* Corresponding authors.

E-mail addresses: wjw@nju.edu.cn (J. Wei), drdingyitao@sina.com.cn (Y. Ding), yudecai@nju.edu.cn (D. Yu).

1. Introduction

Hepatocellular carcinoma (HCC) is one of the most aggressive cancers with a poor prognosis [1]. Recently, there is emerging evidence to reveal the presence of liver cancer stem cells (CSCs) within liver cancer [2–4]. The progression of HCC involves the gradual loss of differentiated phenotypes and acquisition of stemness properties [5]. Stemness of cancer cells is largely responsible for tumor recurrence, metastasis, and chemoresistance, which is the major hurdles for tumor treatment [6,7], but finding effective measures to eradicate CSCs remains a major challenge. Determining the metabolic features of CSCs might therefore discover clinical targets and provide opportunities for more effective therapies.

Research in context

Evidence before this study

Glutaminase 1 (GLS1), which converts glutamine to glutamate, plays a key role in cancer cell metabolism, growth, and proliferation. Previous studies have described that GLS1 was upregulated in HCC. Inhibition of GLS1 reduces the proliferation rate, suppresses epithelial-mesenchymal transition (EMT) process *in vitro*, slows down the tumor growth in several types of cancer cell xenografts, and diminishes cell-autonomous tumorigenesis *in vivo*. GLS1 is being explored as a cancer therapeutic target. Clinical trials of the GLS1 inhibitors in leukemia and solid tumors are ongoing. Cancer stem cells (CSCs) are largely responsible for tumor recurrence and metastasis. However, the role of GLS1 in CSCs was not yet determined in hepatocellular carcinoma (HCC).

Added value of this study

We demonstrated that both KGA and GAC (two splice forms of GLS1) were mitochondrial matrix protein and upregulated in HCC. GAC isoform predicts a poor prognosis. High expression of GLS1 is associated with stemness phenotype and advanced clinicopathological features in HCC. Moreover, GLS1 is highly expressed in liver CSCs, and targeting glutamine metabolism or GLS1 suppresses CSC properties. Wnt/ β -catenin pathway promotes GLS1 expression, and GLS1 regulates stemness properties in HCC *via* ROS/Wnt/ β -catenin signaling. Targeting GLS1 inhibits tumorigenicity *in vivo* of HCC cell xenografts.

Implications of all the available evidence

This study has provided evidence that targeting GLS1 attenuates stemness properties in HCC by increasing ROS and suppressing Wnt/ β -catenin pathway. Thus, GLS1 served as a therapeutic target for elimination of CSCs.

Glutamine is an abundant and versatile nutrient that participates in energy formation, macromolecular synthesis, signaling, and provides NADPH (nicotinamide adenine dinucleotide phosphate) and GSH (glutathione) to maintain redox homeostasis [8]. Glutaminolysis begins with its conversion to glutamate catalyzed by the glutaminases (GLS), which exist as two isozymes in mammalian cells named GLS1 and GLS2 [9]. Through alternative splicing, GLS1 mRNA can give rise to two isoforms that differ only in their C-terminal regions, with the longer form named KGA and the shorter form being called GAC [10]. It was reported that GLS1 functions as a tumor promoter in many cancer types, while GLS2 seems to act as a tumor suppressor [11,12]. In our previous studies, we found the expression of GLS2 was switched to GLS1 during hepatic malignant progression towards HCC, and that GLS1 contributed to the migration and invasion of HCC cells [13,14]. GLS1 regulates antioxidant defense function in cells by increasing GSH levels and decreasing reactive oxygen species (ROS) levels, which in turn protects cells from oxidative stress. Silencing GLS1 expression or inhibiting GLS1 activity perturbed the redox homeostasis of cancer cells [15–17].

Hyperactivation of Wnt/ β -catenin signaling pathway has been identified as one of the most frequent events occurring in CSCs [18]. Activation of the pathway leads to stabilization and nuclear translocation of β -catenin and eventually transcriptional upregulation of target genes [19]. Notably, the Wnt/ β -catenin pathway is heavily implicated in liver CSCs [20,21].

Although there is so far no consensus on the metabolic phenotype of CSCs [22], it is widely accepted that low amounts of ROS were critical for

maintaining the characteristics of CSCs. Increasing evidence now suggests the tight control of mitochondrial ROS production in CSCs is a prerequisite for maintaining their stemness and high fidelity [23–25]. Enlightened by the concept “ROS kill CSCs” and the pivotal role of GLS1 in ROS defense, we speculated that targeting GLS1 might attenuate stem cell-like properties.

In this report, we provide evidence that both KGA and GAC isoforms are exclusively located in the mitochondria matrix and upregulated in HCC. By a series of bioinformatics analyses and functional assays, we demonstrated that GLS1 expression is positively associated with stemness phenotype in HCC and that targeting GLS1 inhibits CSC markers expression and stem-like properties *in vitro* and *in vivo*. Mechanistically, glutamine deprivation or GLS1 inhibition leads to an increased accumulation of ROS, which suppresses the translocation of β -catenin from the cytoplasm to the nucleus and consequently decreases the expression of stemness-related genes.

2. Materials and methods

2.1. Clinical samples

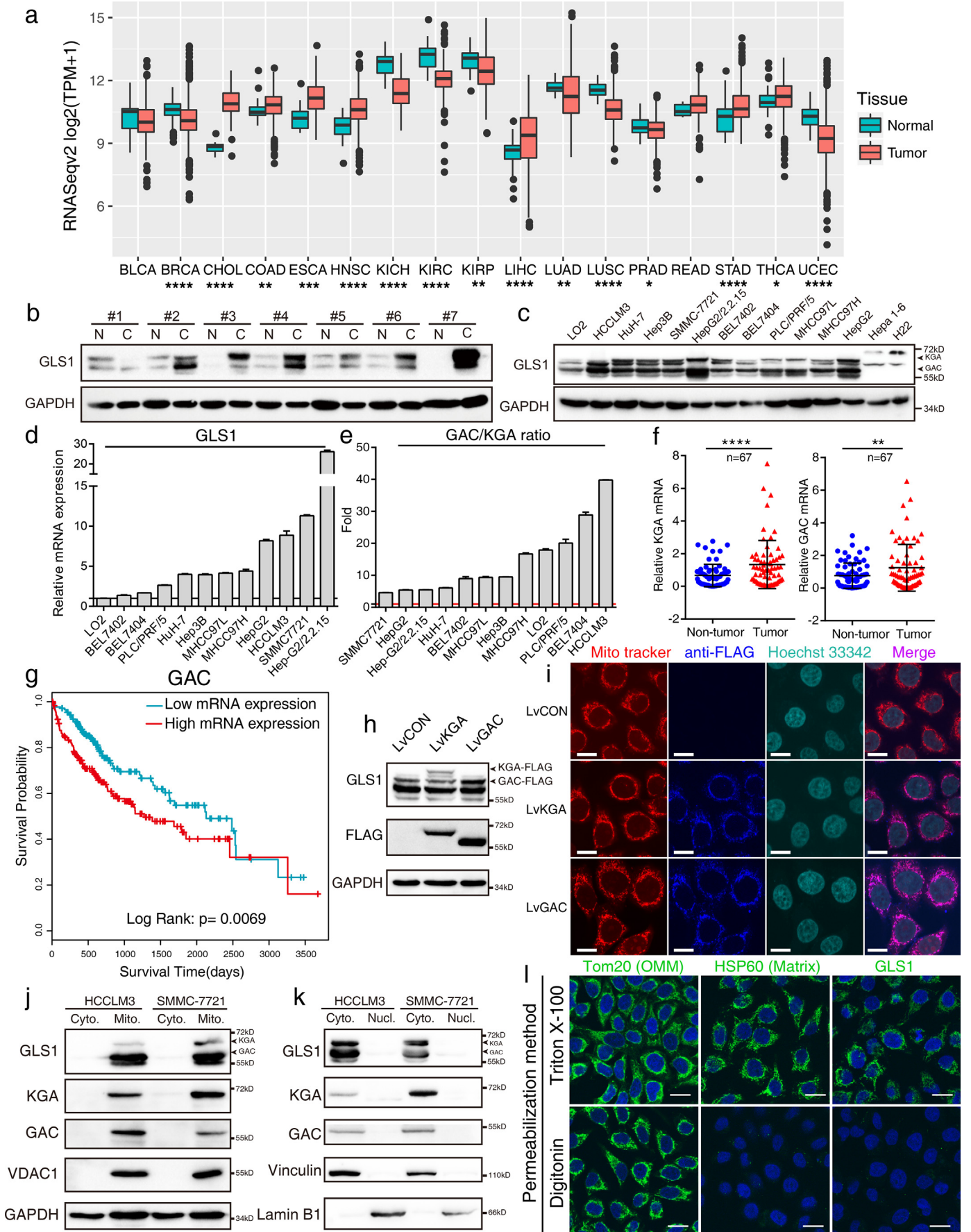
The paired tumor and adjacent non-tumor tissues used in this study were collected under the permissions of patients with HCC undergoing partial hepatectomy in the Department of Hepatobiliary Surgery of Drum Tower Hospital. Informed consent was obtained from all patients. All experimental protocols were approved by the research ethics committee of Drum Tower hospital and research ethics approval for this project was granted from the same institution.

2.2. Cell culture and reagents

The human HCC cell line HCCLM3 and mouse HCC cell line H22 were obtained from the China Center for Type Culture Collection, and the human HCC cell line MHCC97H, HepG2 and mouse HCC cell line Hepa1–6 were obtained from the Cell Bank of Type Culture Collection Chinese Academy of Sciences. The human cell lines LO2, HuH-7, Hep3B, SMMC-7721, HepG2/2.2.15, PLC/PRF/5, MHCC97L, BEL7402 and BEL7404 were provided by Dr. Yong Yang (China Pharmaceutical University, Nanjing, China). HCCLM3, HuH-7, Hep3B, SMMC-7721, HepG2/2.2.15, BEL7402, BEL7404, MHCC97H, HepG2, and mouse HCC cell line Hepa1–6 were cultured in DMEM supplemented with 10% fetal bovine serum, 100 U/mL penicillin and 100 μ g/ml streptomycin (all from ThermoFisher, NY, USA), while the normal human hepatic cell line LO2 and the human HCC cell lines PLC/PRF/5, MHCC97L and the mouse HCC cell line H22 were cultured in RPMI 1640 medium supplemented with 10% fetal bovine serum (FBS) and antibiotics. Cells were maintained at 37 °C in a humidified atmosphere with 5% CO₂. All cell lines were routinely tested for mycoplasma negativity and maintained in culture for a maximum of 20 passages (two months). The compound 968 (#352010) was purchased from Millipore (MA, USA). SKL2001 (#S8320) and BPTES (#S7753) were purchased from Selleck (Shanghai, China). The DMEM without glutamine (#11960044) was purchased from ThermoFisher. The N-Acetyl-L-cysteine (NAC, #A9165), Dimethyl 2-oxoglutarate (DM- α -KG, #349631), and Digitonin (#D141) were obtained from Sigma-Aldrich (MO, USA).

2.3. Lentiviral infection

The lentivirus carrying KGA or GAC isoform or CRISPR/Cas9 virus vector targeting GLS1 were purchased from GeneChem (Shanghai, China). A triple FLAG-tag was engineered at the carboxyl terminus of KGA and GAC construct. Lentiviruses-carrying overexpression or knock-out elements were used to infect the LO2, HCCLM3, Hep3B, and SMMC-7721 according to the manufacturer's protocol. The infected cells were selected with puromycin treatment.



2.4. Sphere formation and colony formation assay

For sphere formation assay, 1000 cells were seeded in Ultra Low Attachment 6-well plates and cultured in DMEM/F12 supplemented with B27, N-2, 20 ng/ml EGF and 20 ng/ml bFGF (all from ThermoFisher). The cell spheres were incubated for two weeks and then examined under a light microscope. For colony formation assay, HCC cells were seeded in twelve-well plates at a density of 500 cells per well and cultured at 37 °C for 1–2 weeks. At the end of the incubation, colonies were stained with crystal violet solution (containing 0.1% crystal violet, 20% methanol, and 80% phosphate buffered saline) for 30 min. Wells were rinsed with water followed by air drying and the colonies were counted. Each measurement was performed in triplicate.

2.5. Western blot

Total proteins were isolated using RIPA lysis buffer (#P0013C, Beyotime Biotechnology, Shanghai, China) and qualified by BCA detecting kit (#P0012, Beyotime Biotechnology) following the manufacturer's protocol. Equal amounts of protein were separated by SDS-PAGE and electrophoretically transferred onto a PVDF membrane (#03010040001, Roche), then blocked with 5% nonfat milk in Tris-buffered saline for one hour at room temperature. The membrane was incubated with specific primary antibodies at 4 °C overnight, followed by incubation with appropriate horseradish peroxidase-conjugated secondary antibodies for one hour at room temperature. Signals were detected using an enhanced chemiluminescence reagent (#WBKLS0500, Millipore, MA, USA) and subjected to a Chemiluminescent detection system (ChamChem 610, Sage Creation Science, Beijing, China). The primary antibodies used were: anti-GLS1 (#ab156876, 1:1000, Abcam), anti-c-MYC (#ab32072, 1:1000, Abcam), anti-KLF4 (#ab215036, 1:1000, Abcam), anti-GAPDH (#ab32072, 1:1000, Santa Cruz Biotechnology), anti-FLAG (#F1804, 1:1000, Sigma-Aldrich), anti-VDAC1 (#10866-1-AP, 1:1000, Proteintech), anti-KGA (#20170-1-AP, 1:1000, Proteintech), anti-GAC (#19958-1-AP, 1:1000, Proteintech), anti-OCT4 (#2750, 1:1000, Cell Signaling Technology), anti-SOX2 (#11064-1-AP, 1:1000, Proteintech), anti-β-Catenin (#8480, 1:1000, Cell Signaling Technology), anti-NANOG (#14295-1-AP, 1:1000, Proteintech), anti-Vinculin (#26520-1-AP, 1:1000, Proteintech), and anti-Lamin B1 (#12987-1-AP, 1:1000, Proteintech).

2.6. Immunohistochemistry (IHC)

Immunohistochemistry was performed as previously described¹³. Briefly, specimens were paraffin-embedded. Serial 4 μm sections were cut, deparaffinized, blocked, and incubated at 4 °C overnight with the primary antibody, followed by horseradish peroxidase-labeled secondary antibody. The primary antibodies used in this study were: rabbit polyclonal antibody to KGA (#20170-1-AP, 1:800, Proteintech), and rabbit polyclonal antibody to GAC (#19958-1-AP, 1:500, Proteintech).

2.7. RNA isolation and quantitative real-time PCR

Total RNA of cells was extracted by TRIZOL (#15596-026, ThermoFisher), and was reverse-transcribed using PrimeScript™ RT Master Mix (#DRR036A, Takara, Shiga, Japan). Quantitative real-time PCR was performed using FastStart Universal SYBR® Green Master (#04913914001, Roche) on the Real-Time PCR system (Applied Biosystems ViiA™ 7 Real-Time PCR System, Foster, CA, USA). The relative expression was normalized to β-actin by the 2^{-ΔΔCt} method. The primer sequences are listed in Table S1.

2.8. Mitochondrial isolation and nuclear-cytoplasmic fractionation

Mitochondria were isolated using a Cell Mitochondria Isolation Kit (#C3601, Beyotime Biotechnology, Shanghai, China) according to the manufacturer's instructions. VDAC1 was treated as a mitochondria control. Nuclear/cytoplasmic fractionation was conducted by the Nucleo-protein Extraction Kit (#C500009, Sangon, Shanghai, China) according to the manufacturer's protocols.

2.9. Flow cytometry analysis

Trypsin digested cells were washed with PBS, followed by incubation with antibodies. The anti-CD13 (#12-0138-41) and isotype (#12-4714-81) antibodies were obtained from eBioscience (ThermoFisher). Samples were subjected to a flow cytometer (FACSCalibur, BD Biosciences) and data were analyzed by a FlowJo software (Version 7.6.5).

2.10. Confocal immunofluorescence

The cells were cultured in glass coverslip bottomed chambers (#154526, ThermoFisher) to 50–80% confluence. After washed with PBS for three times, cells were stained with MitoTracker Red (#M7512, Invitrogen) at a concentration of 100 nM for 20 min at 37 °C. The cells were rinsed with PBS twice, fixed with 4% paraformaldehyde at 25 °C for 10 min, and permeabilized with 1% Triton X-100 or digitonin (50 mg/ml) in PBS at 25 °C for 15 min. Triton X-100 (1%) permeabilizes both the outer mitochondrial membrane (OMM) and inner mitochondrial membrane (IMM), but digitonin (50 mg/ml) permeabilizes only the OMM. Triton X-100 permeabilization is required to detect mitochondrial matrix proteins by immunofluorescence, whereas digitonin permeabilization cannot detect the signal [26].

After washing with PBS, the cells were incubated with primary antibody at 4 °C overnight. The primary antibody used were: anti-GLS1 (#ab156876, 1:100, Abcam), anti-TOM20 (#11802-1-AP, 1:100, Proteintech), anti-HSP60 (#15282-1-AP, 1:100, Proteintech), anti-β-Catenin (#51067-2-AP, 1:100, Proteintech) and anti-FLAG (#F1804, 1:100, Sigma). Cells were washed with PBS three times and incubated with a fluorescent dye-conjugated secondary antibody at room temperature for 1 h. After washed with PBS, cells were stained with DAPI or Hoechst 33342 for 10 min. Then, cells were observed under

Fig. 1. Expression levels and localization of the GLS1 isoforms. (a) Pan-cancer analysis of GLS1 expression across cancers from TCGA. Cancer types with >10 paired normal samples were included in the analysis. The boxplot displays the first quartile, median, and the third quartile of the data. Abbreviations: BLCA: Bladder urothelial carcinoma; BRCA: Breast invasive carcinoma; CHOL: Cholangiocarcinoma; COAD: Colon adenocarcinoma; ESCA: Esophageal carcinoma; HNSC: Head and neck squamous cell carcinoma; KICH: Kidney chromophobe; KIRC: Kidney renal clear cell carcinoma; KIRP: Kidney renal papillary cell carcinoma; LIHC: Liver hepatocellular carcinoma; LUAD: Lung adenocarcinoma; LUSC: Lung squamous cell carcinoma; PRAD: Prostate adenocarcinoma; READ: Rectum adenocarcinoma; STAD: Stomach adenocarcinoma; THCA: Thyroid carcinoma; UCEC: Uterine corpus endometrial carcinoma. (b) Western blot analysis of GLS1 expression in HCC and matched non-tumor tissues. N: normal liver tissue; C: cancer tissue. See also Fig. S1a. (c) Western blot analysis of GLS1 expression in HCC cell lines. (d) The expression levels of GLS1 mRNA in HCC cell lines. (e) The GAC/KGA mRNA ratio in HCC cell lines. (f) Relative mRNA levels of KGA and GAC isoforms in 67 pairs of HCC and matched non-tumorous tissues. (g) High expression of GAC predicts a poor prognosis based on TCGA dataset. (h) HCCLM3 cells stably expressing KGA (IvKGA) or GAC (IvGAC) or empty vector (IvCON) were established using lentiviral approach, then the cell clones derived from single cells were detected for gene expression with FLAG-tag antibody. (i) KGA and GAC location was confirmed by immunofluorescence of HCCLM3 cells stained with FLAG-tag antibody, MitoTracker and Hoechst 33342. Scale bars: 20 μm. (j) The mitochondrial location of KGA and GAC were confirmed by Western blot. (k) Cytoplasmic and nuclear fractions of HCCLM3 and SMMC-7721 cells were isolated to analyze the subcellular location of GLS1. Antibodies to Lamin B1 and vinculin were used as a marker for nuclear and cytoplasmic fractions. (l) Immunofluorescence using anti-Tom20 (OMM protein), anti-HSP60 (Matrix protein), and anti-GLS1 antibodies following permeabilization with 50 μg/mL digitonin or 1% Triton X-100 were shown of HCCLM3 cells. Cells were counterstained with DAPI to show the cell nucleus (blue). Scale bars: 20 μm. Data are presented as mean ± SD. *, *p* < .05; **, *p* < .01; ***, *p* < .001; ****, *p* < .0001.

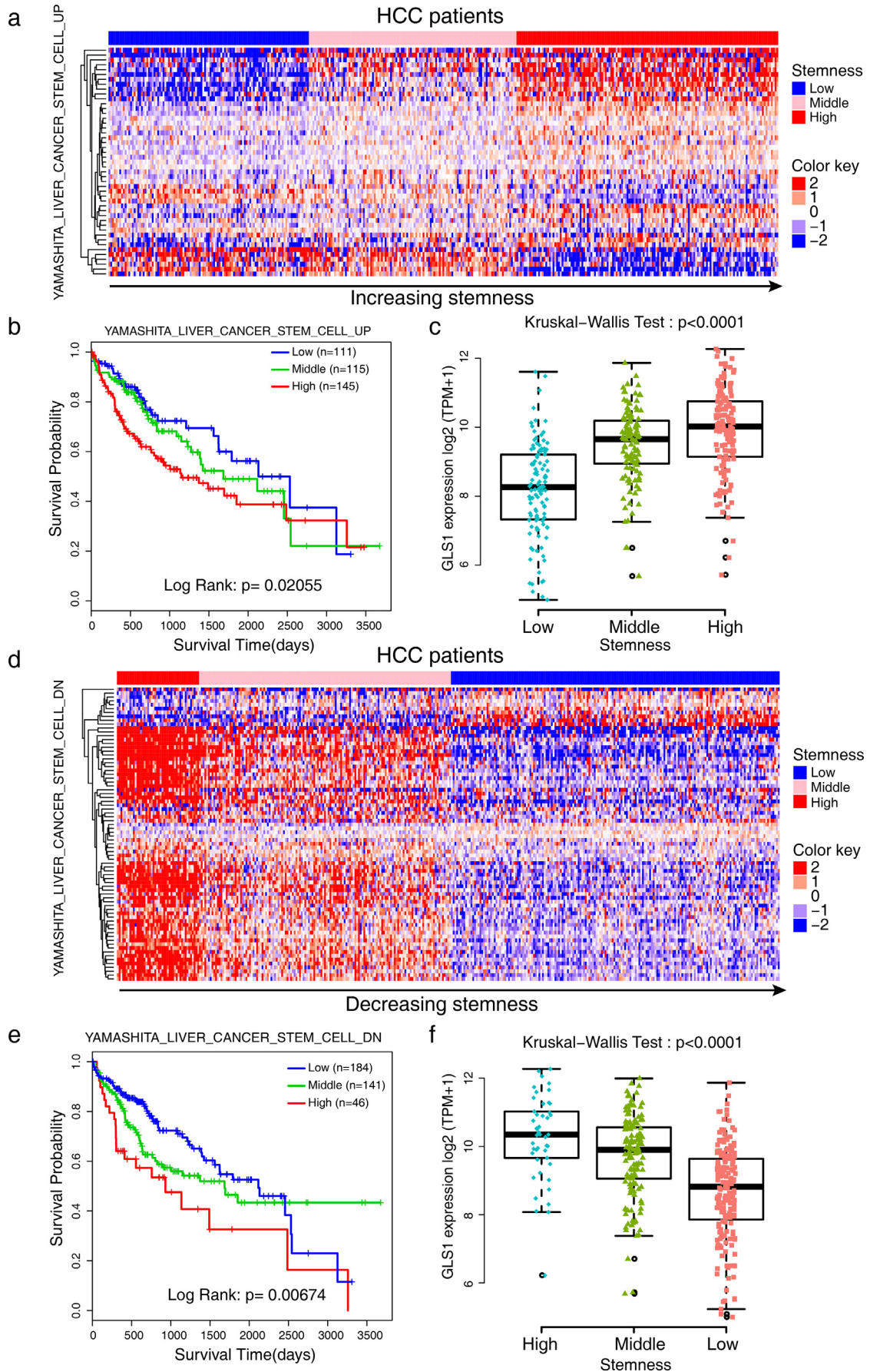


Table 1
Correlations between GLS1 or stemness phenotype and clinicopathological characteristics based on TCGA cohort.

Characteristics	GLS1 expression			Stemness phenotype			
	Low	High	p-value	Low	Middle	High	p-value
Age (years)			0.008*				p < .0001*
Mean	61.71	57.17		62.84	60.64	55.86	
SD	11.41	15.04		11.73	12.18	14.98	
Gender			0.001*				0.001*
Male	140 (75.7%)	110 (59.1%)		85 (76.6%)	84 (73.0%)	81 (55.9%)	
Female	45 (24.3%)	76 (40.9%)		26 (23.4%)	31 (27.0%)	64 (44.1%)	
Patient weight			p < .0001*				p < .0001*
Mean	75.39	70.23		75.43	78.5	66.12	
SD	17.96	20.61		18.34	20.28	17.7	
AFP			0.001*				p < .0001*
<200 µg/L	117 (80.7%)	84 (63.2%)		80 (90.9%)	76 (86.4%)	45 (44.1%)	
≥200 µg/L	28 (19.3%)	49 (36.8%)		8 (9.1%)	12 (13.6%)	57 (55.9%)	
Child Pugh grade			0.796				0.084
a	122 (90.4%)	95 (91.3%)		79 (86.8%)	66 (97.1%)	72 (90.0%)	
b/c	13 (9.6%)	9 (8.7%)		12 (13.2%)	2 (2.9%)	8 (10.0%)	
Tumor weight			0.02*				0.276
Mean	249.28	363.63		235.32	300.1	366.34	
SD	346.85	505.05		272.85	386.02	554.5	
Vital status			0.378				0.042*
Alive	123 (66.5%)	118 (63.4%)		81 (73.0%)	76 (66.1%)	84 (57.9%)	
Dead	62 (33.5%)	68 (36.6%)		30 (27.0%)	39 (33.9%)	61 (42.1%)	
Histologic grade			0.012*				p < .0001*
G1	33 (17.9%)	22 (12.1%)		27 (24.8%)	19 (16.7%)	9 (6.3%)	
G2	97 (52.7%)	80 (44.0%)		54 (49.5%)	63 (55.3%)	60 (42.0%)	
G3/4	54 (29.3%)	80 (44.0%)		28 (25.7%)	32 (28.1%)	74 (51.7%)	
Pathological stage			0.049*				0.013*
Stage I	97 (55.7%)	74 (42.8%)		59 (54.6%)	57 (56.4%)	55 (39.9%)	
Stage II	39 (22.4%)	47 (27.2%)		27 (25.0%)	21 (20.8%)	38 (27.5%)	
Stage III/IV	38 (21.8%)	52 (30.1%)		22 (20.4%)	23 (22.8%)	45 (32.6%)	
T stage			0.026*				0.008*
T1	102 (55.4%)	79 (42.9%)		61 (55.5%)	63 (55.8%)	57 (39.3%)	
T2	41 (22.3%)	53 (28.8%)		27 (24.5%)	25 (22.1%)	42 (29.0%)	
T3/4	41 (22.3%)	52 (28.3%)		22 (20.0%)	25 (22.1%)	46 (31.7%)	
Vascular invasion			0.802				0.043*
No	107 (66.0%)	99 (64.7%)		71 (71.7%)	68 (69.4%)	67 (56.8%)	
Yes	55 (34.0%)	54 (35.3%)		28 (28.37%)	30 (30.6%)	51 (43.2%)	

* Statistically significant.

FLUOVIEW FV10i confocal microscope (Olympus, Tokyo, Japan) and images were analyzed using FV10-ASW 4.0 Viewer (Olympus).

2.11. ROS generation detection

Intracellular ROS accumulation was determined by a ROS assay kit (#S0033, Beyotime Biotechnology) that utilizes DCFH-DA as a fluorescent probe. After drug treatments, cells were incubated with 10 µM DCFH-DA for 20 min at 37 °C and then were washed with DMEM for three times. Then the DCF fluorescence distribution was detected by flow cytometry or confocal microscopy.

2.12. Metabolomic analysis

HCCLM3 cells were treated with 5 µM 968 for two weeks, then subjected to an LC-MS/MS spectrometer analysis to determine the metabolic changes. The cell protein's extraction, separation, and identification were performed in Shanghai Applied Protein Technology (Shanghai, China).

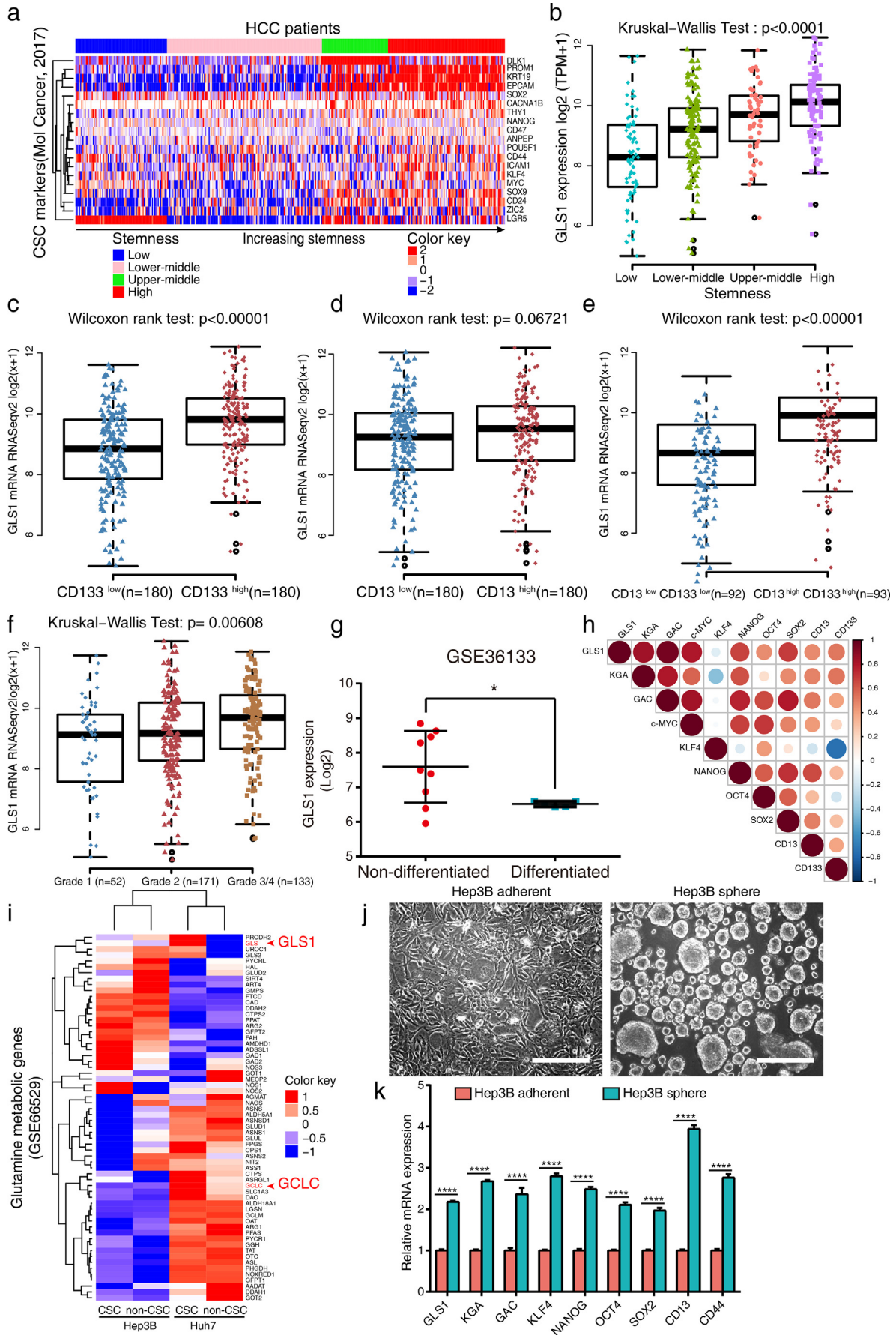
2.13. Animal studies

Male BALB/c nude mice (6 weeks old) were obtained from the Model Animal Research Center of Nanjing University (Nanjing, China). All experimental procedures using animals were in accordance with the guidelines provided by the Animal Ethics Committee of the Affiliated Drum Tower Hospital of Medical School of Nanjing University. HCCLM3 or SMMC-7721 cells with stable GLS1 knockout (GLS1 KO) or the corresponding blank vector (WT) were subcutaneously injected into each flank of the nude mice. Tumor growth was determined by measuring the short and long diameter of the tumor with a caliper every three days. 5–6 weeks after injection, the mice were sacrificed. Tumor volume was calculated according to the formula volume = (width² × length)/2.

2.14. Bioinformatics analysis

The RNA-seq and clinical data of different cancer categories (up to Jan 28, 2016) were retrieved from the TCGA database (<https://gdc.cancer.gov>). The microarray datasets (GSE36133, GSE25097, GSE62044, and GSE66529) were downloaded from the GEO (<http://>

Fig. 2. Unsupervised consensus clustering uncovers the correlation between GLS1 and stemness phenotype based on TCGA dataset. (a) Heatmap presented the expression profile of YAMASHITA UP gene set that positively correlated with hepatic cancer stem cell-like traits. Subgroups identified by YAMASHITA UP gene set have an increased expression of stemness-related genes from left to right. (b) Kaplan-Meier survival analysis of patients in subgroups generated by consensus clustering. (c) The average expression level of GLS1 in subgroups identified by YAMASHITA UP gene set. (d) Heatmap presented the expression profile of YAMASHITA DN gene set that negatively correlated with hepatic stem cell features. Subgroups identified by the YAMASHITA DN gene set have a decreased stemness from left to right. (e) Kaplan-Meier survival analysis of patients in subgroups with different stemness levels in HCC. (f) The average expression level of GLS1 in subgroups identified by the YAMASHITA DN gene set. The boxplot displays the minimum, first quartile, median, third quartile, and maximum of the data.



www.ncbi.nlm.nih.gov/geo/). Three previously reported stemness-related gene sets were downloaded from the Molecular Signatures Database (MSigDB) including “WONG EMBRYONIC STEM CELL CORE” (abbreviated as WONG CORE) [27], “YAMASHITA LIVER CANCER STEM CELL UP” (abbreviated as YAMASHITA UP) and “YAMASHITA LIVER CANCER STEM CELL DN” (abbreviated as YAMASHITA DN) [28]. Unsupervised consensus clustering analysis was carried out to discover different clusters with varying stemness as previously described [29]. Briefly, ConsensusClusterPlus was utilized to identify robust clusters. K-mean approach with the Euclidean distance we used to perform consensus clustering. The procedure was run 1000 iterations with maxK = 6, and a sub-sampling ratio of 0.8. Heatmaps were generated by Bioconductor package complexHeatmap. To analyze the pathway gene expression level, average gene expression is calculated for all involved genes for one sample, and the average value represents this sample's average gene expression of the pathway. The expression level of GLS1 in HCC cell lines was analyzed in GSE36133 dataset, in which 10 cell lines were non-differentiated HCC cell lines (HLE, HLF, JHH-6, SK-HEP-1, SNU-182, SNU-387, SNU-398, SNU-423, SNU-449, and SNU-475) and 5 cell lines were differentiated HCC cell lines (C3A, Hep 3B2.1–7, HepG2, HuH-6, and HuH-7) [30].

2.15. Statistical analysis

The quantitative data were analyzed with Student's *t*-test or Mann-Whitney *U* test. The paired *t*-test or Wilcoxon signed-rank test were used for paired samples to make a statistical comparison between groups. The count data were analyzed with Pearson Chi-Square. The Kruskal-Wallis test or Mann-Whitney *U* test was used for ranked data as appropriate. The repeated measures ANOVA was used to compare the difference of the tumor volume in different groups. Survival curves were estimated by the Kaplan-Meier method. The log-rank test was used to determine the statistical differences between survival curves. All testing was carried out using Prism 6.0 (GraphPad, San Diego, USA) or SPSS (Version 23.0, Chicago, USA) or R (Version 3.4.0, Auckland, NZ). The two-sided *p*-value < .05 was defined as statistically significant for all statistical analyses. The data were plotted as mean ± standard deviation (SD).

3. Results

3.1. The mitochondrial matrix protein GLS1 (both KGA and GAC) is highly expressed in HCC, and GAC predicts a poor prognosis

Both our previous study and results from other group have demonstrated that GLS1 expression was markedly increased in HCC samples [13,16]. To gain a systematical expression profile of GLS1, we analyzed its expression pattern across cancers based on TCGA datasets. GLS1 was constitutively highly expressed in kidney and was significantly up-regulated in bile ducts, colon, esophageal, head and neck, liver, stomach, and thyroid cancers (Fig. 1a). We tested the expression level of GLS1 in HCC with 20 pairs of clinical tissues. GLS1 was highly expressed in most HCC tissues, as compared with the peri-tumor tissues (Fig. 1b, Fig. S1a). We also found that GLS1 was elevated in most HCC cell lines (Fig. 1c–d).

The GLS1 antibody recognized two or more bands (Fig. 1c, Fig. S1b). We clarified the bands with isoform-specific antibodies: GAC (58 kDa) and KGA (65 kDa) (Fig. S1c). We calculated the GAC/KGA ratio among

HCC cell lines. GAC was found to be the predominant isoform in HCC cell lines (Fig. 1e). Both KGA and GAC isoforms are upregulated in our clinical tissues (Fig. 1f), and a microarray dataset downloaded from GEO (GSE25097; Fig. S1d–e). IHC staining with isoform-specific antibodies further validated that both KGA and GAC protein levels are increased in HCC (Fig. S1f). In a recent study, a negative correlation between KGA and GAC was reported in colon cancer³¹. However, we obtained significant direct associations between KGA and GAC mRNA expression in nontumor tissue and HCC tissues from our clinical samples and the two microarray datasets (GEO: GSE62044, GSE25097; Fig. S2a–d). High expression levels of GAC mRNA, but not KGA isoform indicated a poor prognosis of HCC based on TCGA dataset (Fig. 1g, Fig. S2e).

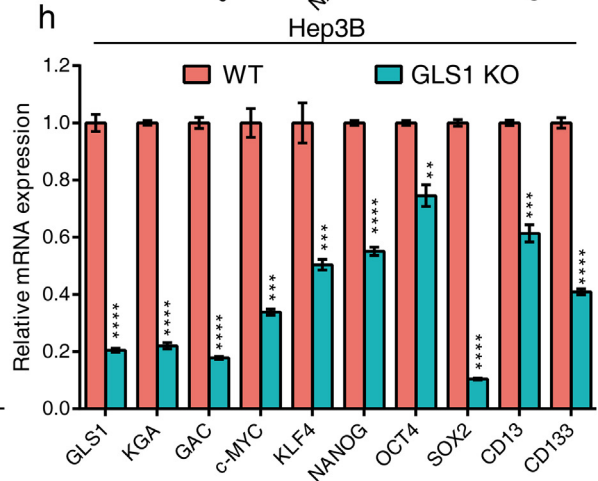
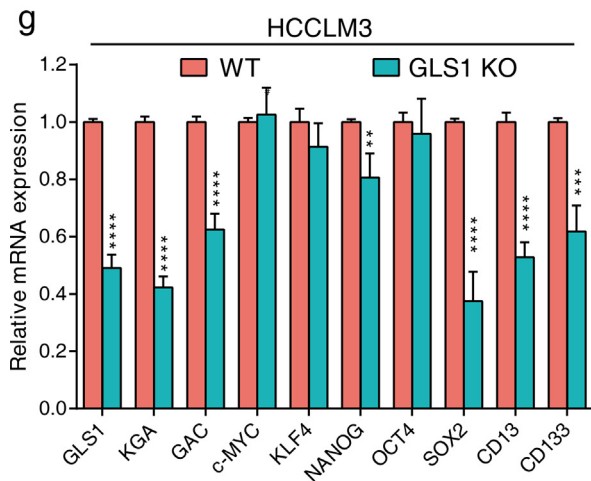
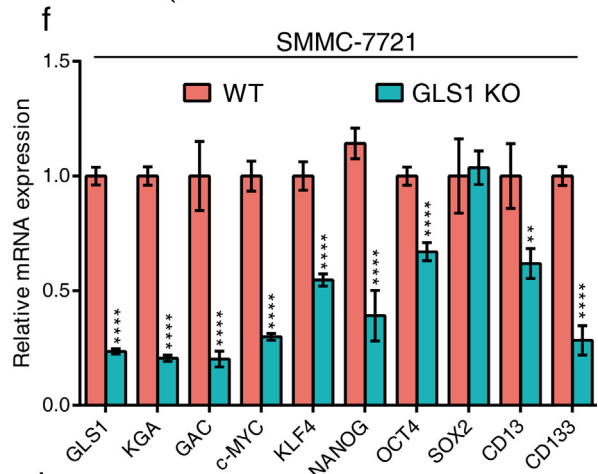
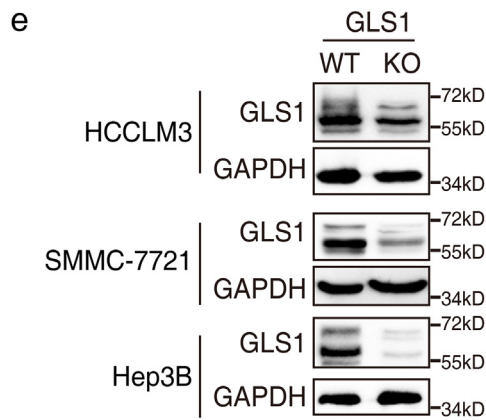
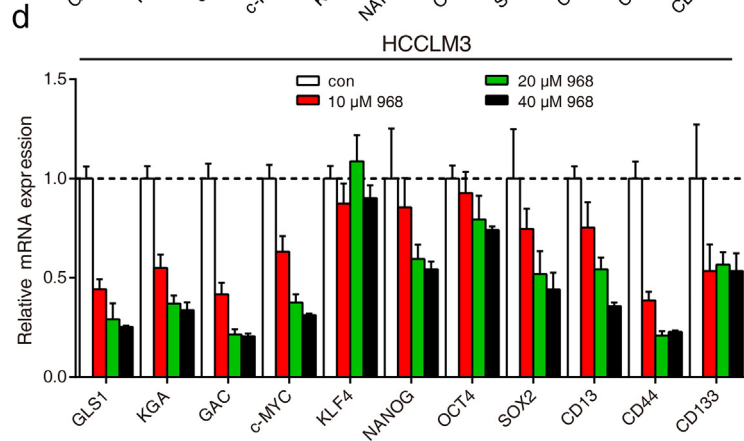
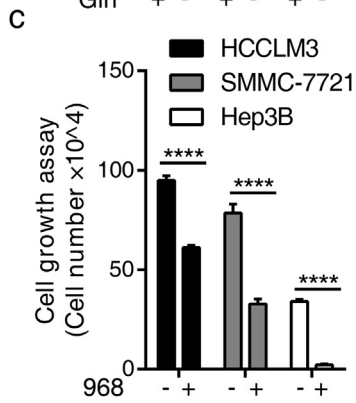
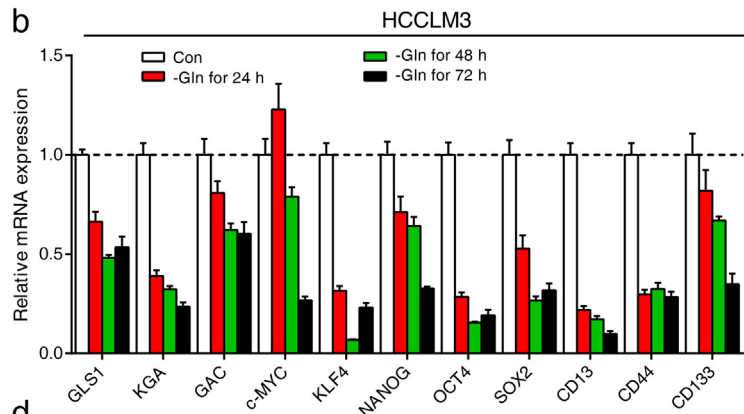
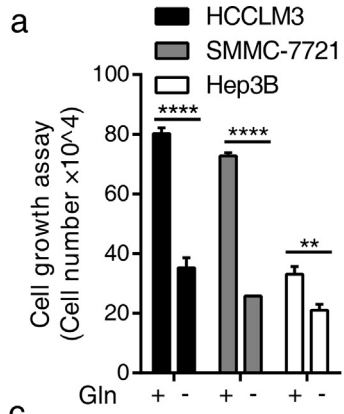
The subcellular localization of GLS1 isoform was controversial [11]. It was reported that GAC is the only isoform present in the mitochondria, while KGA is localized in the cytosol [32]. We performed immunofluorescence with GLS1 antibody in HCCLM3 and SMMC-7721 cell lines and observed that GLS1 was located in the mitochondria (Fig. S2f). Furthermore, we established stable cell lines overexpressing KGA or GAC with FLAG-tag at their C termini by lentiviral (Fig. 1h). Immunofluorescence with FLAG-tag antibody further confirmed that both KGA and GAC isoforms are present in the mitochondria (Fig. 1i). We then fractionated cell lysates into their nuclear, cytoplasmic, and mitochondrial compartments and blotted with GLS1 or isoform-specific antibodies. Western blot showed that both KGA and GAC are exclusively expressed in the mitochondria (Fig. 1j–k).

To further determine the submitochondrial location of GLS1, we immunostained HCCLM3 cells with distinct permeabilization methods (See Methods). Tom20 (an OMM protein) and HSP60 (a matrix protein) were clearly recognized by their respective antibodies after permeabilization with Triton X-100. Meanwhile, permeabilization with digitonin was insufficient to allow detection of the matrix protein HSP60. Anti-GLS1 immunoreactivity was absent from cells after permeabilization with digitonin, but became detectable following Triton X-100 permeabilization (Fig. 1l). This observation demonstrated that GLS1 is a mitochondrial matrix protein, and that glutaminolysis of HCC cells occurs exclusively within the mitochondrial matrix.

3.2. High expression of GLS1 is associated with stemness phenotype and advanced clinicopathological features in HCC

It has been reported that glutamine plays a significant role in maintaining the stemness of lung cancer [33], and that inhibiting GLS1 suppresses stemness properties in head and neck squamous carcinoma [34]. To investigate the association between GLS1 and stemness phenotype in HCC, we downloaded three well-established gene sets related to stemness from the MSigDB and performed consensus clustering in HCC patients from TCGA dataset (See Methods). The YAMASHITA UP gene set includes genes upregulated in liver CSCs, which is positively correlated with stemness phenotype of HCC, whereas the YAMASHITA DN gene set is the opposite. Unsupervised K-means consensus clustering with the YAMASHITA UP gene set recognized three stable subgroups with increasing stemness (Fig. 2a, Fig. S3a). High expression of stemness genes was associated with a poor clinical outcome (Fig. 2b) and an increased expression of GLS1 (Fig. 2c). Similar results were also obtained from the YAMASHITA DN gene set. Consensus clustering generated three clusters with varying stemness (Fig. 2d, Fig. S3b). Patients with

Fig. 3. GLS1 is highly expressed in liver CSCs. (a) Consensus clustering uncovered four subgroups with the liver-specific CSC markers. (b) GLS1 displayed gradually elevated RNA expression with the increased expression of liver CSC markers. (c) GLS1 is highly expressed in CD133^{high} HCC samples. HCC samples were divided into two subpopulations according to CD133 expression levels, followed by analyzing the expression of GLS1. (d) GLS1 is highly expressed in CD133^{high} HCC samples. (e) GLS1 is highly expressed in CD133^{high} CD133^{high} HCC samples. (f) The expression of GLS1 increased gradually with the progress of tumor grade. (g) GLS1 is highly expressed in non-differentiated HCC cell lines compared to differentiated HCC cell lines from GSE36133. (h) The correlations between GLS1 and CSC markers were validated by qRT-PCR in 12 HCC cell lines. The correlation coefficient was shown by colour, in which red indicated a positive correlation and blue indicated a negative correlation. (i) The GSE66529 dataset was analyzed to obtain the expression profile of glutamine metabolic genes in CSCs and non-CSCs. GLS1 and GCLC were indicated by the arrows. (j) Representative photographs of the adherent Hep3B cells and Hep3B sphere. Scale bars: 50 μm. (k) Increased expression of GLS1 and CSC markers in oncospheres derived from Hep3B. Data are presented as mean ± SD. The boxplot displays the minimum, first quartile, median, third quartile, and maximum of the data. *, *p* < .05; ****, *p* < .0001.



the highest stemness had the worst prognosis (Fig. 2e) and the highest expression of GLS1 (Fig. 2f). We then calculated the average gene expression of the aforementioned gene sets and analyzed their correlations with GLS1. GLS1 is positively associated with the YAMASHITA UP gene set (Fig. S3c), but negatively correlated to the YAMASHITA DN gene set (Fig. S3d). We further validated the results with the WONG CORE gene set which consists of the genes upregulated in embryonic stem cells. In agreement, high stemness was associated with poor survival and high expression of GLS1 (Fig. S4a–d). Taken together, these data indicated that GLS1 is associated with stemness phenotype of HCC.

We further explored the associations between the expression levels of GLS1 or stemness-related genes and clinicopathological characteristics of HCC based on TCGA dataset (Table 1). The high GLS1 expression is associated with higher AFP level ($p = .001$; Mann-Whitney *U* test), tumor weight ($p = .02$; Mann-Whitney *U* test), advanced histological stages ($p = .012$; Kruskal-Wallis test), T stage ($p = .026$; Kruskal-Wallis test) and pathological stages ($p = .049$; Kruskal-Wallis test). Interestingly, we also found that patients with high GLS1 expression tended to be female ($p = .001$; Pearson Chi-Square), younger age ($p = .008$; Mann-Whitney *U* test) and low body weights ($p < .0001$; Mann-Whitney *U* test). Similarly, high expression of stemness-related genes (identified by YAMASHITA UP gene set in Fig. 2a) was related to higher AFP level ($p < .0001$; Kruskal-Wallis test), higher survival rate ($p = .042$; Kruskal-Wallis test), advanced histological stages ($p < .0001$; Kruskal-Wallis test), T stage ($p = .008$; Kruskal-Wallis test) and pathological stages ($p = .013$; Kruskal-Wallis test), and more vascular invasion ($p = .043$; Kruskal-Wallis test). We also determined that patients with high stemness tended to be younger ($p < .0001$; Kruskal-Wallis test), females ($p = .001$; Pearson Chi-Square) with low body weights ($p < .0001$; Kruskal-Wallis test). These results demonstrated that upregulation of GLS1 or stemness-related genes was associated with advanced clinicopathological features of HCC.

3.3. GLS1 is highly expressed in liver CSCs, and targeting glutamine metabolism or GLS1 suppresses CSC properties

To explore the expression pattern of GLS1 in liver CSCs, we performed consensus clustering with 19 liver-specific CSC markers reviewed by Kouki et al. [35]. Four subgroups with increasing stemness were obtained, in which the expression of GLS1 gradually increased correspondingly (Fig. 3a–b, Fig. S4e). The expression levels of GLS1 was positively correlated with CD13 and CD133 in HCC samples (Fig. 3c–e). In addition, GLS1 expression was significantly increased with advancing tumor grade, indicated high GLS1 expression was associated with dedifferentiation (Fig. 3f). To validate this observation, we further analyzed the expression of GLS1 in differentiated and non-differentiated HCC cell lines (GEO: GSE36133). GLS1 was significantly highly expressed in non-differentiated HCC cell lines (Fig. 3g). We performed qRT-PCR to validate the correlations between the expression of GLS1 and CSC markers in HCC cell lines and identified that GLS1 was directly associated with most CSC markers (Fig. 3h). KLF4 tended to be inversely correlated with other CSC markers possibly due to the limited sample size. We further analyzed GLS1 expression in CD13⁺CD133⁺ cells (liver CSCs) and CD13[−]CD133[−] cells (non-CSCs) in a microarray dataset (GEO: GSE66529), and found that GLS1 was highly expressed in liver CSCs (Fig. 3i). We next tested the expression levels of GLS1 in oncosphere cells (Fig. 3j). GLS1 together with multiple core stem cell genes (KLF4, NANOG, OCT4, SOX2, CD13, and CD44) were dramatically elevated in sphere cultures (Fig. 3k). Overall, these data indicated that GLS1 is highly expressed in liver CSCs.

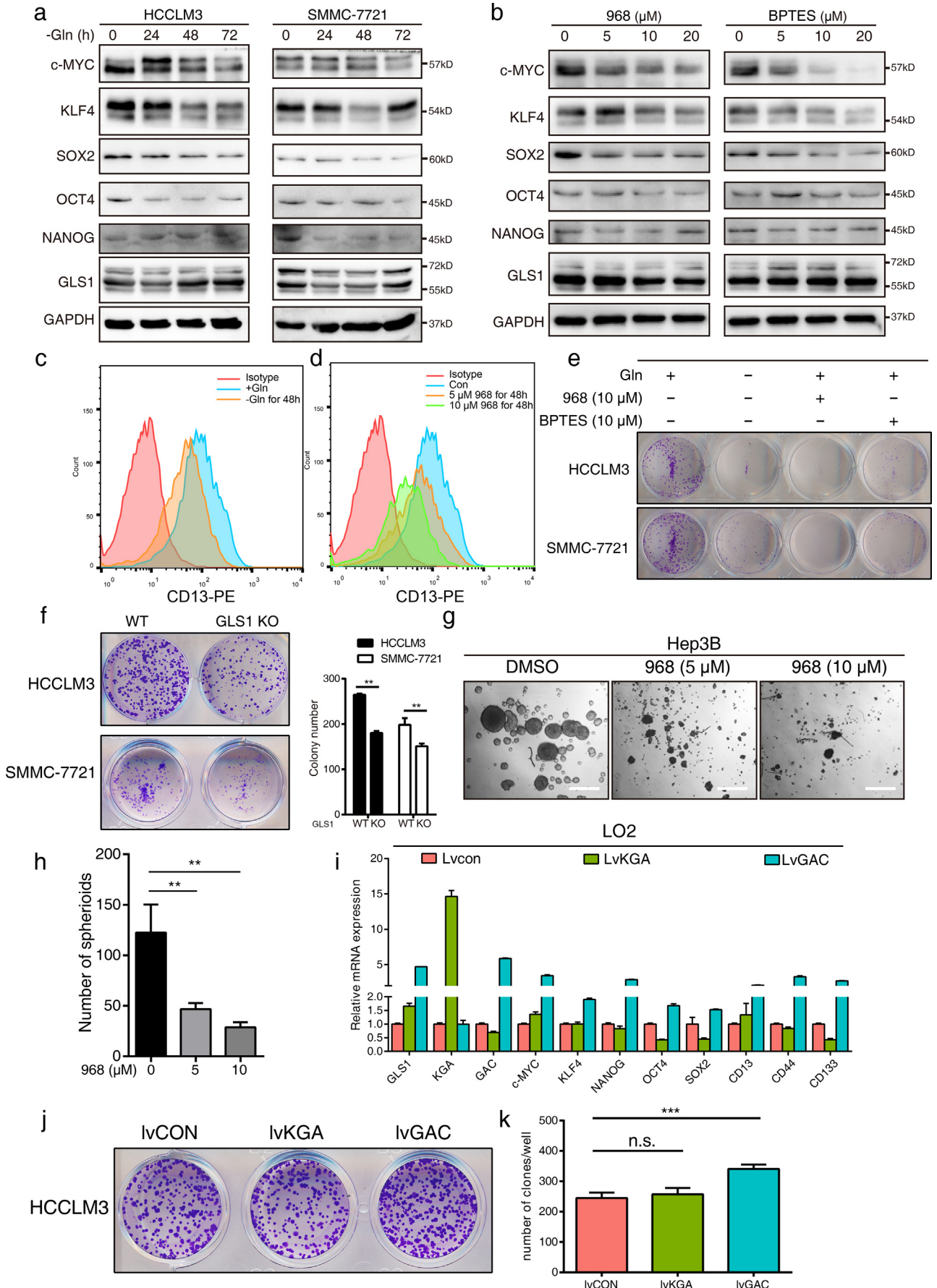
To determine the importance of glutamine metabolism on HCC cells, we cultured HCC cell lines (HCCLM3, SMMC-7721, and Hep3B) in the presence or absence of glutamine. Glutamine withdrawal inhibited the growth of HCC cell lines (Fig. 4a) and suppressed the expression of CSC markers in HCCLM3 (Fig. 4b). We treated HCC cells with previously reported GLS1-specific inhibitor 968 [36], and observed apparent inhibitory effects on the growth HCC cell lines (Fig. 4c). Similarly, 968 treatment inhibited the expression of CSC markers (Fig. 4d). We further employed a lentiviral-based CRISPR/Cas9 knockdown approach to suppress GLS1 expression in HCCLM3, SMMC-7721 and Hep3B HCC cells (Fig. 4e). Upon silencing of GLS1, we observed a downregulation of well-characterized stemness markers including c-MYC, KLF4, NANOG, OCT4, SOX2, CD13, and CD133, as compared with wild-type (WT) control HCC cell lines (Fig. 4f–h).

Furthermore, we suppressed the glutamine metabolism and analyzed the expression of CSC markers by Western blot. Deprivation of glutamine inhibited the expression of CSC markers including NANOG, OCT4, KLF4, SOX2, and c-MYC in HCCLM3 and SMMC-7721 cell lines (Fig. 5a). Similarly, treatment HCC cell lines with GLS1 inhibitors (968 or BPTES) suppressed the expression of CSC markers (Fig. 5b). Consistent with the above-mentioned results, withdrawal of glutamine or 968 treatment reduced the expression of CD13 as measured by flow cytometry (Fig. 5c–d). On the other hand, deprivation of glutamine or 968 treatment dramatically inhibited the colony formation ability of HCCLM3 and SMMC-7721 cell lines (Fig. 5e). Knockout of GLS1 with CRISPR/Cas9 system markedly inhibited the colony formation in the aforementioned cells (Fig. 5f). Treatment Hep3B cells with 968 impaired the sphere formation ability (Fig. 5g–h). To explore which isoform was responsible for the stemness in HCC cell lines, we established stable cell lines overexpressing KGA or GAC, respectively. Overexpression of GAC rather than KGA increased the expression of CSC markers (Fig. 5i) and the colony formation ability (Fig. 5j–k). Collectively, our data suggested that targeting glutamine metabolism or GLS1 suppresses CSC properties and GAC might play a more important role than KGA isoform.

3.4. Wnt/ β -catenin pathway promotes GLS1 expression, and GLS1 regulates stemness properties in HCC via ROS/Wnt/ β -catenin signaling

We next seek to further elucidate the molecular mechanism of GLS1 in regulating stemness. GLS1 is a mitochondrial matrix protein, which indicated GLS1 might exhibit its function not in a protein-protein interaction manner, but through its metabolic products. Since low ROS level was critical for maintaining stemness, we speculated that GLS1 might influence stemness through redox signaling. In addition, we noticed Glutamate-Cysteine Ligase Catalytic Subunit (GCLC), the first rate-limiting enzyme of glutathione synthesis, was highly expressed in CSCs (Fig. 3i). Deprivation of glutamine or 968 treatment increased the intracellular ROS level as measured by both flow cytometry and immunofluorescence (Fig. 6a–b). Consistently, GLS1 was negatively correlated with reactive oxygen species pathway (Fig. S5a). Hydrogen peroxide (H_2O_2), one form of ROS, markedly inhibited the clonogenic formation of HCCLM3 cells (Fig. 6c) and decreased the expression of CSC markers such as c-MYC and KLF4 (Fig. 6d). Glutamate, the product of the GLS1 reaction, is a precursor of GSH which acts as the major cellular antioxidant. Glutamate is also the major source of α -ketoglutarate (α -KG), a TCA cycle intermediate participating in energy formation (Fig. 6e). To further explore the metabolites responsible for the suppression of stemness properties by targeting GLS1, we performed a rescue experiment. Supplement of *N*-acetyl-L-cysteine (NAC), a ROS scavenger, rather than dimethyl α -ketoglutarate (DM- α -KG), a cell-permeable

Fig. 4. GLS1 expression is associated with stemness in HCC. (a) HCC cells (HCCLM3, SMMC-7721, and Hep3B) were cultured in the presence or absence of glutamine for 72 h before cells were trypsinized and counted. (b) HCCLM3 were cultured in DMEM with glutamine withdraw for 24, 48, or 72 h. qRT-PCR was performed to detect the stemness markers. (c) HCC cells were cultured in the presence or absence of 10 μ M 968 for 72 h before cells were trypsinized and counted. (d) HCCLM3 were treated with the indicated concentration of 968 for 48 h, then the expression levels of CSC markers were analyzed by qRT-PCR. (e) Cell lines with stable knockout of GLS1 were established using a CRISPR/Cas9 system. Knockout of GLS1 in SMMC-7721 (f), HCCLM3 (g) and Hep3B (h) downregulated the expression of stemness genes. Data are presented as mean \pm SD. **, $p < .01$; ***, $p < .001$; ****, $p < .0001$.



analog of α -KG, could rescue the colony formation of HCCLM3 cells under the glutamine deprivation or 968 treatment condition (Fig. 6f). These data together suggested that GLS1 regulates stemness through redox balance. We also performed a metabolomics analysis to determine the metabolic changes responsible for GLS1 inhibition. The concentrations of metabolites such as adenosine, cytosine, uridine, and cytidine decreased, UMP and AMP, precursors for the synthesis of nucleotides, accumulated significantly in 968 treated cells, suggesting impairment of DNA synthesis (Fig. 6g, Table S2).

Previous studies have revealed Wnt/ β -catenin signaling pathway plays a central role in maintaining the stemness of HCC [20,21]. Consistent with that, we found increasing stemness accompanied high expression of Wnt/ β -catenin pathway (Fig. S5b), whereas decreasing stemness coupled with the low expression of Wnt/ β -catenin pathway (Fig. S5c). Considering that hydrogen peroxide inhibited the expression of both β -catenin and CSC markers (Fig. 6d), we speculated that GLS1 might influence stemness through β -catenin. Thus, we further investigated the relationship between GLS1 and β -catenin. Firstly, we performed gene set enrichment analysis (GSEA) and correlation analysis to analyze the association of GLS1 and Wnt/ β -catenin pathway. Both analyses revealed that GLS1 was significantly associated with Wnt/ β -catenin pathway (Fig. 6h, Fig. S5d). Secondly, we activated Wnt/ β -catenin pathway with its agonist SKL2001 [37] and examined GLS1 levels. Both GLS1 mRNA and protein were upregulated after SKL2001 treatment (Fig. 6i–j, Fig. S7a). Using the Wnt target gene list, we found that transcripts that were upregulated by Wnt/ β -catenin pathway almost invariably correlated positively with GLS mRNA levels (Fig. S6). Collectively, these results indicate that Wnt/ β -catenin pathway promotes GLS1 expression.

Upon Wnt/ β -catenin activation, β -catenin accumulates in the cytoplasm and then translocates to the nucleus, where it engages DNA-bound TCF transcription factors and activates target genes [19]. Interestingly, many of the CSC markers (such as CD44, OCT4, SOX2 and NONOG) are direct Wnt targets [38]. SKL2001 treatment increased the expression of CSC markers and other Wnt target genes (such as CCND1, BIRC5, BCL2, and AXIN2) in HCCLM3 cells (Fig. S7b). We sought to examine whether GLS1 regulates stemness properties through the Wnt/ β -catenin pathway. 968 treatment decreased the mRNA expression of β -catenin and Wnt target genes (Fig. 6k). In addition, Withdrawal of glutamine or targeting GLS1 with 968 or BPTES reduced the total protein levels of β -catenin (Fig. S7c). Further, we separated the nuclear and cytoplasmic protein. Targeting GLS1 reduced both the cytoplasmic and nuclear β -catenin. SKL2001 increased the cytosolic and nuclear β -catenin, which could be partly abrogated by GLS1 inhibitors or glutamine withdrawal (Fig. 6l, Fig. S7d–e). Similarly, GLS1 knockout decreased the nuclear β -catenin and reduced the agonist effect of SKL2001 to Wnt/ β -catenin pathway (Fig. 6m). To validate this results, we performed immunofluorescence assay. While SKL2001 treatment increased the expression of β -catenin, both glutamine withdrawal and GLS1 inhibitors reduced the expression of cytosolic and nuclear β -catenin (Fig. S8). Taken together, these results suggested that GLS1 regulates stemness properties in HCC via ROS/Wnt/ β -catenin signaling.

3.5. Targeting GLS1 inhibits tumorigenicity *in vivo*

We then explored the effects of GLS1 on tumorigenicity potential *in vivo*. HCCLM3 and SMMC-7721 cells stably overexpressing the

control plasmid (WT) or CRISPR/Cas9 vector targeting GLS1 (GLS1 KO) were injected into the right and left flanks of nude mice, respectively. We observed a slower tumor growth in the GLS1 KO group. The mice injected with GLS1 KO cell lines exhibited a significantly smaller tumor size than those injected with control cells both in HCCLM3 cells (Fig. 7a–c) and SMMC-7721 cells (Fig. 7d–f). The knockout efficiency of GLS1 was validated by Western blot in SMMC-7721 cells (Fig. 7g). We further reduced the SMMC-7721 cells number injected subcutaneously into nude mice. GLS1 knockout decreased the tumor-initiating capacity *in vivo* compared with the control cells (Fig. 7h). These observations proved that targeting GLS1 could inhibit tumorigenicity *in vivo*.

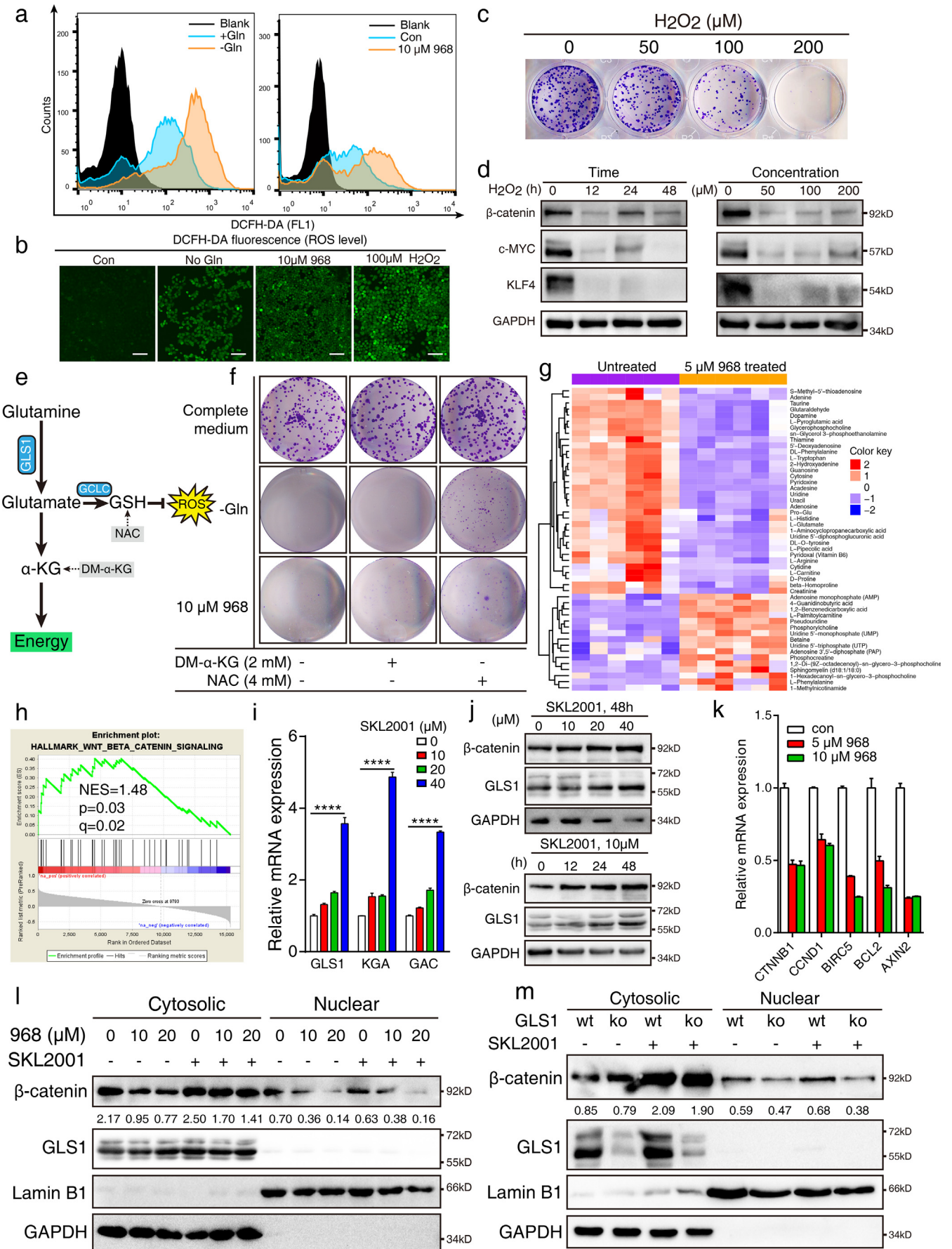
In summary, we present evidence that GLS1 plays a significant role in maintaining the stemness of HCC by ROS/Wnt/ β -catenin signaling pathway, and targeting GLS1 attenuates stemness properties in HCC *in vitro* and *in vivo*, which indicated that GLS1 might be a therapeutic target to eliminate CSCs (Fig. 7i).

4. Discussion

Liver cancer is a highly lethal disease that typically has a poor prognosis. Liver CSCs are considered to be responsible for liver cancer initiation, metastasis, relapse, and chemoresistance. In the current study, by means of a series of bioinformatics analyses and functional assays, we unraveled the regulatory role of GLS1 in stemness phenotype of HCC. We delineated that GLS1 mediates HCC stemness through Wnt/ β -catenin signaling and that GLS1 serves as a therapeutic target for suppressing CSC properties.

GLS1 consists of two isoforms named KGA and GAC. Although KGA and GAC share the same active site, they have different catalytic capabilities with KGA being less catalytically active. KGA was found in the cytosol but not in the mitochondria, as opposed to GAC. KGA contained three ankyrin repeats in its distinct C-terminus which exclusively functioned to mediate protein-protein interactions [32,39]. These studies indicate KGA may participate in transcription regulation in a non-enzymatic manner. Although it is now well established that GAC is much catalytically active than KGA, the functional difference between KGA and GAC has remained unclear. GAC is reported to be the predominant GLS1 splice variant in lung cancer [40], breast cancer [10], AML [41], colon cancer [31] and gastroenteropancreatic neuroendocrine neoplasms/tumors (GEP-NET) [42]. Higher GAC/KGA ratio bespeaks the fast proliferative phenotype in GEP-NET [42], and high GAC expression combined with low KGA expression had shorter overall survival in colon cancer [31]. Moreover, only the GAC-specific siRNA was able to elicit apoptosis, while the KGA-specific siRNA had no effect in HeLa cells [43]. Together, these studies indicated the more important role of GAC isoform in tumors, and drug-based therapies specifically targeting GAC seem more likely to succeed. Consistent with these findings, we observed GAC is the predominant isoform in HCC cell lines, and is associated with the prognosis and stemness phenotype of HCC patients. Nevertheless, we also noticed the content of KGA is the same or even more as GAC in HCC tissues (Fig. 1b, Fig. S1a), which suggested the relative content of KGA and GAC might be different *in vivo* and *in vitro*. Overall, the difference of the biological function between KGA and GAC is still not yet fully understood. Recently, Pascoal et al. investigated the origin and evolution of human glutaminases from a new genetic evolutionary perspective, and proposed that GAC possibly evolved from the parental KGA

Fig. 5. Targeting GLS1 suppresses cancer stem cell properties. (a) Effect of glutamine on the expression of stemness genes. HCCLM3 and SMMC-7721 were cultured in DMEM with the absence of glutamine for 24, 48, or 72 h. Cell lysates were subjected to Western blot to measure the expression of stemness markers. (b) HCCLM3 cells were treated with 5, 10, or 20 μ M 968 or BPTES for 48 h, then Western blot was employed to detect the expression of stemness markers. (c–d) Glutamine deprivation or 968 treatment for 48 h resulted in a decrease of CD13 expression as evaluated by flow cytometry. (e) Colony formation assay was performed to assess the effect of glutamine withdrawal and GLS1 inhibitors (968 or BPTES) on tumorigenicity. (f) Colony formation assay and quantitative analysis were performed in HCCLM3 and SMMC-7721 cells with GLS1 knockout. (g–h) 968 treatment reduced the number and size of the tumorspheres in Hep3B as measured by sphere-formation assays. Scale bars: 200 μ m (i) The expression changes of stemness markers in cell lines stably overexpressing empty vector (lvCON), KGA (lvKGA) or GAC (lvGAC) isoform by lentiviral. (j–k) Colony formation assay and quantitative analysis were performed in lvCON, lvKGA, and lvGAC cell lines. Data are presented as mean \pm SD. **, $p < .01$; ***, $p < .001$.



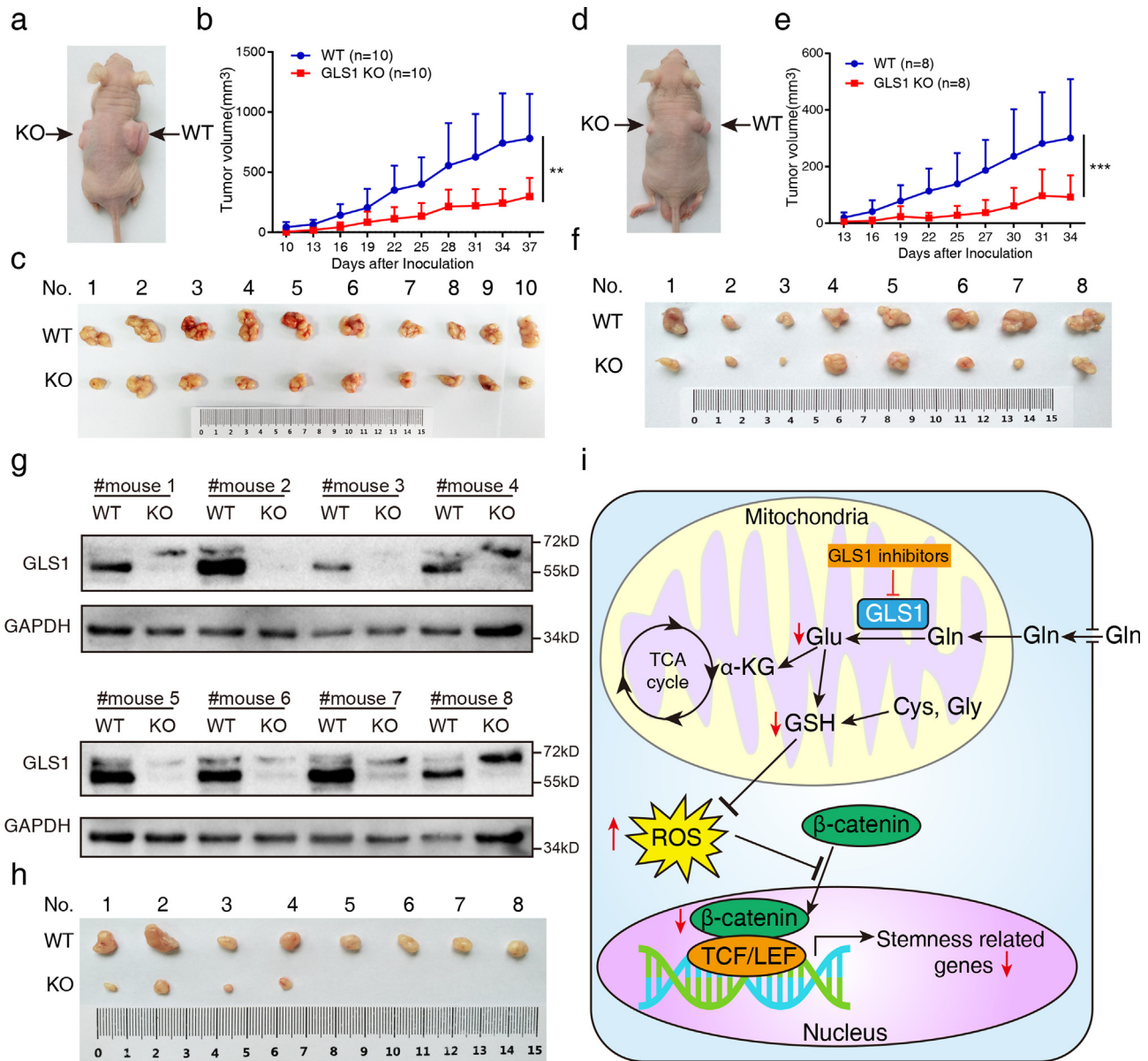


Fig. 7. GLS1 regulates *in vivo* tumorigenicity. 2×10^6 of HCCLM3 (a–c) and SMMC-7721 (d–f) stable cell lines were subcutaneously inoculated into both flanks of nude mice, with GLS1 knockout on the left flanks, and wide-type cells on the right flanks. Tumor volumes were monitored every three days. Five weeks after the injection, mice were photographed and tumors were collected. Representative tumor images and tumor growth curves are shown. The tumors volumes were analyzed by the repeated measures ANOVA. Data are presented as mean \pm SD. ** $P < .01$, *** $p < .001$. (g) The tumors isolated from nude mice were subjected to Western blot to validate the GLS1 knockout efficiency. (h) 5×10^5 of GLS1 KO or wide-type SMMC-7721 cells were subcutaneously inoculated into both flanks of nude mice. Mice were sacrificed after six weeks postinoculation and tumors samples were collected. (i) Schematic model illustrating the effect of GLS1 on Wnt/β-catenin signaling and stemness in HCC. Targeting GLS1 triggers an increase of ROS, attenuates nuclear translocation of β-catenin and subsequent inhibits the β-catenin target genes, leading to the suppression of CSC properties in HCC. Abbreviations: Gln, Glutamine; GSH, Glutathione; Glu, Glutamate; Cys, Cysteine; Gly, Glycine; ROS, Reactive oxygen species; TCF/LEF, T-cell factor/lymphoid enhancer factor.

to create a more active enzyme, because the lack of ankyrin repeats enhances the catalytic efficiency of KGA [44], which might deepen our understanding of functional diversity of GLS1 isoforms.

The acquisition and maintenance of stemness are increasingly recognized as a metabolism-dependent process [45]. Thus, the metabolic features of CSCs represent a promising target for elimination of CSCs. Over

Fig. 6. GLS1 regulates CSC properties via ROS/Wnt/β-catenin signaling. Determination of cellular ROS in HCCLM3 cells. Cells were cultured with glutamine deprivation or $10 \mu\text{M}$ 968 for 48 h, and ROS was detected using DCFH-DA by flow cytometry (a) or confocal (b). H_2O_2 was used as positive control. Scale bars: $100 \mu\text{m}$. (c) Colony formation assay was performed on HCCLM3 cell line treated with indicated concentration of H_2O_2 . (d) H_2O_2 treatment suppressed the expression of KLF4, c-MYC, and β-catenin. (e) Simplified schematic of the glutamine metabolism pathways. (f) HCCLM3 cells were assayed for colony formation in complete DMEM medium or without glutamine or in the presence of $10 \mu\text{M}$ 968 alone or together with 2 mM DM-α-KG or 4 mM NAC. (g) HCCLM3 cells were treated with $5 \mu\text{M}$ 968 for two weeks, then metabolomic analysis was performed to screen for the differentially expressed metabolites. (h) Genes associated with GLS1 were analyzed by gene set enrichment analysis (GSEA) based on TCGA dataset. Wnt/β-catenin pathway was enriched. (i) HCCLM3 was treated with the indicated concentration of SKL2001 for 24 h, then GLS1 mRNA expression was examined. (j) HCCLM3 cells were treated with the indicated concentration of SKL2001 for 48 h (upper panel) or treated with $10 \mu\text{M}$ SKL2001 for 12, 24, and 48 h (lower panel), then GLS1 protein expression was measured. (k) HCCLM3 cells were treated with different concentration of 968 for 24 h. The mRNA levels of β-catenin (CTNNB1) and its target genes (CCND1, BIRC5, BCL2, and AXIN2) were determined by q-PCR. (l) HCCLM3 cells were pretreated with 10 or $20 \mu\text{M}$ 968 for 24 h, then treated with SKL2001 for another 24 h. Cells were harvested and fractionated into cytoplasmic and nuclear fractions, thereafter the expression of GLS1, β-catenin protein levels were determined by Western blot. GAPDH and lamin B1 were detected as fractionation and loading controls. (m) SMMC-7721 cells with stable knockout of GLS1 by CRISPR/Cas9 was treated with SKL2001 for 24 h, then cytoplasmic and nuclear fractions were prepared and subjected to Western blot with anti-GLS1 and anti-β-catenin antibodies. Data are presented as mean \pm SD. ****, $p < .0001$.

the past years, the metabolic phenotype of CSCs has been extensively investigated. CSCs have been described as primarily glycolytic or preferentially relying on OXPHOS in a tumor type-dependent manner. However, there is so far no consensus on this [22,46]. Glycolysis was shown to be the preferred metabolic pattern of liver CSC, and stem cell marker NANOG represses OXPHOS and mitochondrial ROS in liver CSCs [47]. In our study, we identified that glutamine depletion or targeting GLS1 suppressed CSC traits in HCC, which seemed to be inconsistent with the metabolic phenotype of HCC characterized by low mitochondrial respiration and high glycolytic activity. This inconsistency may be due to glutamine also plays a vital role in clearing ROS besides in satisfying bioenergetic demands and macromolecular synthesis. Low amounts of ROS are needed to maintain quiescence and the self-renewal potential of CSCs. Consistent with the antioxidant stress role of glutamine metabolism, we found NAC rather than DM- α -KG could restore the colony formation ability of HCCLM3 cells under the glutamine deprivation or 968 treatment condition (Fig. 6e). Thus, our study emphasizes the important role of glutamine in counteracting ROS and maintaining redox homeostasis in liver CSCs and that redox balance is a key function of GLS1 in liver CSCs.

In our experiments, we observed both KGA and GAC isoforms are exclusively expressed in the mitochondria matrix. Targeting GLS1 has a similar effect as glutamine deprivation on stemness phenotype, which indicated that GLS1 is less likely to participate in transcription regulation by physically interacting with other proteins but through its metabolic products to regulate stemness. In the circumstances, we performed metabolomics analysis seek to determine the metabolites that link GLS1 and stemness. Most differential expressed products are nucleic acid metabolism-related metabolites, suggesting impairment of DNA synthesis. The NAC only had a slight rescue effect. A possible explanation for this might be that glutamine is an important precursor for nucleic acid synthesis, which could not be replaced by ROS scavenger. We failed to find a novel metabolite that associated with stemness from the metabolomics results possibly limited by the quality of mass spectrometry. Similarly, Han et al. revealed inhibition of GLS1 caused an accumulation of NAD⁺ in their mass spectrometric analysis, suggesting an increase of oxidative stress in the condition of GLS1 repression [48]. In addition, previous studies have described glutamine withdrawal or targeting GLS1 is associated with an increase of ROS levels [49–53]. We validated that glutamine depletion or repressing GLS1 caused an accumulation of ROS, which sequentially suppressed the translocation of β -catenin to the nucleus. This finding is consistent with a study that ROS decreases the amount of nuclear β -catenin [54].

The linkage between glutamine metabolism and Wnt/ β -catenin pathway has already established in the liver. Three genes involved in glutamine metabolism encoding glutamine synthetase (GS), ornithine aminotransferase, and the glutamate transporter-1 are all targets of Wnt/ β -catenin signaling [55,56]. It has been reported that Wnt3a induced GLS1 expression in a β -catenin-dependent manner in breast cancer cell lines [57]. In this study, we found that GLS1 is regulated by, and regulates Wnt/ β -catenin pathway. To the best of our knowledge, the present investigation has demonstrated, for the first time, that GLS1 regulates β -catenin and that glutamine metabolism is essential for the activation of the Wnt/ β -catenin pathway. Thus, our findings here contribute to expanding our understanding of the role of Wnt/ β -catenin in glutamine metabolism and hepatocarcinogenesis.

GLS1 inhibitors are already ongoing in clinical trials, which might limit the novelty of applicable outcome of our findings. However, this study has provided evidence that targeting GLS1 attenuates stemness properties in HCC by increasing ROS and suppressing Wnt/ β -catenin pathway and that GLS1 served as a therapeutic target for elimination of CSCs. We think this study might not only facilitate us to understand the antitumor mechanism of GLS1 inhibitors and but also provide an experimental basis for the expansion of clinical indications of GLS1 inhibitors to improve the clinical management of HCC.

Funding sources

This work was supported by grants from the Nature Science Foundation of China (No. 81871967), Social Development Foundation of Jiangsu Province of China (No. BE2018604), the Jiangsu Provincial Natural Science Foundation (BK20151094), Jiangsu Provincial Medical Talent, the Nanjing Science and Technology Project (No. 201803028) and the Fundamental Research Funds for the Central Universities (YG1805016 021414380375)

Authors' contributions

YTD, DCY, and WJW conceived and designed experiments. BHL, YJC, GM, LYQ, TCX, CY, OYL, and SHW performed the experiments. BHL performed the bioinformatics analyses. BHL and DCY wrote the manuscript. All authors approved the final version of the manuscript.

Conflict of interest

The authors declare that they have no competing interests.

Acknowledgments

The authors thank the Biobank of Nanjing Drum Tower Hospital for providing the liver cancer specimens. BHL would specifically like to thank his wife-to-be Dan Zhao for her unwavering love and support.

Appendix A. Supplementary data

Supplementary data to this article can be found online at <https://doi.org/10.1016/j.ebiom.2018.11.063>.

References

- [1] Forner A, Reig M, Bruix J. Hepatocellular carcinoma. *Lancet* 2018;391(10127):1301–14.
- [2] Chiba T, Zheng YW, Kita K, et al. Enhanced self-renewal capability in hepatic stem/progenitor cells drives cancer initiation. *Gastroenterology* 2007;133(3):937–50.
- [3] Ma S, Chan KW, Hu L, et al. Identification and characterization of tumorigenic liver cancer stem/progenitor cells. *Gastroenterology* 2007;132(7):2542–56.
- [4] Zhu Z, Hao X, Yan M, et al. Cancer stem/progenitor cells are highly enriched in CD133+CD44+ population in hepatocellular carcinoma. *Int J Cancer* 2010;126(9):2067–78.
- [5] Malta TM, Sokolov A, Gentles AJ, et al. Machine learning identifies stemness features associated with oncogenic dedifferentiation. *Cell* 2018;173(2):338–54 [e15].
- [6] Yamashita T, Wang XW. Cancer stem cells in the development of liver cancer. *J Clin Invest* 2013;123(5):1911–8.
- [7] Chiba T, Kamiya A, Yokosuka O, Iwama A. Cancer stem cells in hepatocellular carcinoma: recent progress and perspective. *Cancer Lett* 2009;286(2):145–53.
- [8] Hensley CT, Wasti AT, Deberardinis RJ. Glutamine and cancer: cell biology, physiology, and clinical opportunities. *J Clin Invest* 2013;123(9):3678–84.
- [9] Aledo JC, Gomez-Fabre PM, Olalla L, Marquez J. Identification of two human glutaminase loci and tissue-specific expression of the two related genes. *Mamm Genome* 2000;11(12):1107–10.
- [10] Elgadi KM, Meguid RA, Qian M, Souba WW, Abcouwer SF. Cloning and analysis of unique human glutaminase isoforms generated by tissue-specific alternative splicing. *Physiol Genomics* 1999;1(2):51–62.
- [11] Katt WP, Lukey MJ, Cerione RA. A tale of two glutaminases: homologous enzymes with distinct roles in tumorigenesis. *Future Med Chem* 2017;9(2):223–43.
- [12] Zhang C, Liu J, Zhao Y, et al. Glutaminase 2 is a novel negative regulator of small GTPase Rac1 and mediates p53 function in suppressing metastasis. *Elife* 2016;5:e10727.
- [13] Yu D, Shi X, Meng G, et al. Kidney-type glutaminase (GLS1) is a biomarker for pathologic diagnosis and prognosis of hepatocellular carcinoma. *Oncotarget* 2015;6(10):7619–31.
- [14] Cao YJ, Li BH, Shi XB, et al. Effects of GLS1 on the epithelial-mesenchymal transition of hepatocellular carcinoma in vitro and in vivo. *Transl Cancer Res* 2018;7(1):97–108.
- [15] Martin-Rufian M, Nascimento-Gomes R, Higuero A, et al. Both GLS silencing and GLS2 overexpression synergize with oxidative stress against proliferation of glioma cells. *J Mol Med* 2014;92(3):277–90.
- [16] Xiang Y, Stine ZE, Xia J, et al. Targeted inhibition of tumor-specific glutaminase diminishes cell-autonomous tumorigenesis. *J Clin Invest* 2015;125(6):2293–306.
- [17] Ulanet DB, Couto K, Jha A, et al. Mesenchymal phenotype predisposes lung cancer cells to impaired proliferation and redox stress in response to glutaminase inhibition. *PLoS One* 2014;9(12):e115144.

- [18] Fodde R, Brabletz T. Wnt/ β -catenin signaling in cancer stemness and malignant behavior. *Curr Opin Cell Biol* 2007;19(2):150–8.
- [19] Clevers H, Nusse R. Wnt/ β -catenin signaling and disease. *Cell* 2012;149(6):1192–205.
- [20] Yamashita T, Budhu A, Forgues M, Wang XW. Activation of hepatic stem cell marker EpCAM by Wnt- β -catenin signaling in hepatocellular carcinoma. *Cancer Res* 2007;67(22):10831–9.
- [21] Yang W, Yan H-X, Chen L, et al. Wnt/ β -catenin signaling contributes to activation of normal and tumorigenic liver progenitor cells. *Cancer Res* 2008;68(11):4287–95.
- [22] Sancho P, Barneda D, Heeschen C. Hallmarks of cancer stem cell metabolism. *Br J Cancer* 2016;114(12):1305–12.
- [23] Kobayashi CI, Suda T. Regulation of reactive oxygen species in stem cells and cancer stem cells. *J Cell Physiol* 2012;227(2):421–30.
- [24] Shi X, Zhang Y, Zheng J, Pan J. Reactive oxygen species in cancer stem cells. *Antioxid Redox Signal* 2012;16(11):1215–28.
- [25] Bigarella CL, Liang R, Ghaffari S. Stem cells and the impact of ROS signaling. *Development* 2014;141(22):4206–18.
- [26] Okatsu K, Kimura M, Oka T, Tanaka K, Matsuda N. Unconventional PINK1 localization to the outer membrane of depolarized mitochondria drives Parkin recruitment. *J Cell Sci* 2015;128(5):964–78.
- [27] Wong DJ, Liu H, Ridky TW, Cassarino D, Segal E, Chang HY. Module map of stem cell genes guides creation of epithelial cancer stem cells. *Cell Stem Cell* 2008;2(4):333–44.
- [28] Yamashita T, Ji J, Budhu A, et al. EpCAM-positive hepatocellular carcinoma cells are tumor-initiating cells with stem/progenitor cell features. *Gastroenterology* 2009;136(3):1012–24.
- [29] Li B, Xu T, Liu C, et al. Liver-enriched genes are associated with the prognosis of patients with hepatocellular carcinoma. *Sci Rep* 2018;8(1):11197.
- [30] Zhu P, Wang Y, He L, et al. ZIC2-dependent OCT4 activation drives self-renewal of human liver cancer stem cells. *J Clin Invest* 2015;125(10):3795–808.
- [31] Redis RS, Vela LE, Lu W, et al. Allele-specific reprogramming of cancer metabolism by the long non-coding RNA CCAT2. *Mol Cell* 2016;61(4):520–34.
- [32] Cassago A, Ferreira AP, Ferreira IM, et al. Mitochondrial localization and structure-based phosphate activation mechanism of Glutaminase C with implications for cancer metabolism. *Proc Natl Acad Sci U S A* 2012;109(4):1092–7.
- [33] Liao J, Liu PP, Hou G, et al. Regulation of stem-like cancer cells by glutamine through beta-catenin pathway mediated by redox signaling. *Mol Cancer* 2017;16(1):51.
- [34] Kamarajan P, Rajendiran TM, Kinchen J, Bermudez M, Danciu T, Kapila YL. Head and neck squamous cell carcinoma metabolism draws on glutaminolysis, and stemness is specifically regulated by glutaminolysis via aldehyde dehydrogenase. *J Proteome Res* 2017;16(3):1315–26.
- [35] Nio K, Yamashita T, Kaneko S. The evolving concept of liver cancer stem cells. *Mol Cancer* 2017;16(1):4.
- [36] Wang JB, Erickson JW, Fujii R, et al. Targeting mitochondrial glutaminase activity inhibits oncogenic transformation. *Cancer Cell* 2010;18(3):207–19.
- [37] Gwak J, Hwang SG, Park HS, et al. Small molecule-based disruption of the Axin/beta-catenin protein complex regulates mesenchymal stem cell differentiation. *Cell Res* 2012;22(1):237–47.
- [38] Takahashi-Yanaga F, Kahn M. Targeting Wnt signaling: can we safely eradicate cancer stem cells? *Clin Cancer Res* 2010;16:3153–62 1078-0432. CCR-09-2943.
- [39] Thangavelu K, Pan CQ, Karlberg T, et al. Structural basis for the allosteric inhibitory mechanism of human kidney-type glutaminase (KGA) and its regulation by Raf-Mek-Erk signaling in cancer cell metabolism. *Proc Natl Acad Sci U S A* 2012;109(20):7705–10.
- [40] van den Heuvel AP, Jing J, Wooster RF, Bachman KE. Analysis of glutamine dependency in non-small cell lung cancer: GLS1 splice variant GAC is essential for cancer cell growth. *Cancer Biol Ther* 2012;13(12):1185–94.
- [41] Jacque N, Ronchetti AM, Larrue C, et al. Targeting glutaminolysis has antileukemic activity in acute myeloid leukemia and synergizes with BCL-2 inhibition. *Blood* 2015;126(11):1346–56.
- [42] Szeliga M, Ćwikła J, Obara-Michlewska M, Cichocki A, Albrecht J. Glutaminases in slowly proliferating gastroenteropancreatic neuroendocrine neoplasms/tumors (GEP-NET): selective overexpression of mRNA coding for the KGA isoform. *Exp Mol Pathol* 2016;100(1):74–8.
- [43] Masamha CP, Xia Z, Peart N, et al. CFIm25 regulates glutaminase alternative terminal exon definition to modulate miR-23 function. *RNA* 2016;22(6):830–8.
- [44] Pasquali CC, Islam Z, Adamoski D, et al. The origin and evolution of human glutaminases and their atypical C-terminal ankyrin repeats. *J Biol Chem* 2017;292(27):11572–85.
- [45] Folmes CD, Terzic A. Energy metabolism in the acquisition and maintenance of stemness. *Semin Cell Dev Biol*. Elsevier; 2016. p. 68–75.
- [46] Peiris-Pages M, Martinez-Outschoorn UE, Pestell RG, Sotgia F, Lisanti MP. Cancer stem cell metabolism. *Breast Cancer Res* 2016;18(1):55.
- [47] Chen CL, Uthaya Kumar DB, Punj V, et al. NANOg metabolically reprograms tumor-initiating stem-like cells through tumorigenic changes in oxidative phosphorylation and fatty acid metabolism. *Cell Metab* 2016;23(1):206–19.
- [48] Han T, Zhan W, Gan M, et al. Phosphorylation of glutaminase by PKC ϵ is essential for its enzymatic activity and critically contributes to tumorigenesis. *Cell Res* 2018;1.
- [49] Gao P, Tchernyshyov I, Chang TC, et al. C-Myc suppression of miR-23a/b enhances mitochondrial glutaminase expression and glutamine metabolism. *Nature* 2009;458(7239):762–5.
- [50] Meng G, Xia M, Xu C, Yuan D, Schnurr M, Wei J. Multifunctional antitumor molecule 5'-triphosphate siRNA combining glutaminase silencing and RIG-I activation. *Int J Cancer* 2014;134(8):1958–71.
- [51] Yuan L, Sheng X, Clark LH, et al. Glutaminase inhibitor compound 968 inhibits cell proliferation and sensitizes paclitaxel in ovarian cancer. *Am J Transl Res* 2016;8(10):4265–77.
- [52] Lora J, Alonso FJ, Segura JA, Lobo C, Marquez J, Mates JM. Antisense glutaminase inhibition decreases glutathione antioxidant capacity and increases apoptosis in *Ehrlich ascitic* tumour cells. *Eur J Biochem* 2004;271(21):4298–306.
- [53] Elgogary A, Xu Q, Poore B, et al. Combination therapy with BPTES nanoparticles and metformin targets the metabolic heterogeneity of pancreatic cancer. *Proc Natl Acad Sci U S A* 2016;113(36):E5328–36.
- [54] Shin SY, Kim CG, Jho E-H, et al. Hydrogen peroxide negatively modulates Wnt signaling through downregulation of β -catenin. *Cancer Lett* 2004;212(2):225–31.
- [55] Cadoret A, Ovejero C, Terris B, et al. New targets of β -catenin signaling in the liver are involved in the glutamine metabolism. *Oncogene* 2002;21(54):8293.
- [56] Sekine S, Lan BYA, Bedolli M, Feng S, Hebrok M. Liver-specific loss of β -catenin blocks glutamine synthesis pathway activity and cytochrome p450 expression in mice. *Hepatology* 2006;43(4):817–25.
- [57] Lee SY, Jeon HM, Ju MK, et al. Dlx-2 and glutaminase upregulate epithelial-mesenchymal transition and glycolytic switch. *Oncotarget* 2016;7(7):7925–39.